Icarus xxx (2015) xxx–xxx

Contents lists available at ScienceDirect

Icarus

journal homepage: www.journals.elsevier.com/icarus

The tectonics of Titan: Global structural mapping from Cassini RADAR

Zac Yung-Chun Liu [a,b,*], Jani Radebaugh [a], Ron A. Harris [a], Eric H. Christiansen [a], Catherine D. Neish [c,d], Randolph L. Kirk [e], Ralph D. Lorenz [f], the Cassini RADAR Team

[a] *Department of Geological Sciences, Brigham Young University, Provo, UT 84602, USA*
[b] *Now at School of Earth and Space Exploration, Arizona State University, Tempe, AZ 85287, USA*
[c] *Department of Earth Sciences, The University of Western Ontario, London, ON N6A 5B7, Canada*
[d] *Centre for Planetary Science and Exploration, The University of Western Ontario, London, ON N6A 5B7, Canada*
[e] *Astrogeology Division, U.S. Geological Survey, Flagstaff, AZ 86001, USA*
[f] *The Johns Hopkins University Applied Physics Laboratory, Laurel, MD 20723, USA*

ARTICLE INFO

Article history:
Received 19 May 2015
Revised 10 October 2015
Accepted 17 November 2015
Available online xxxx

Keywords:
Titan, surface
Satellites, surfaces
Tectonics
Radar observations
Geological processes

ABSTRACT

The Cassini RADAR mapper has imaged elevated mountain ridge belts on Titan with a linear-to-arcuate morphology indicative of a tectonic origin. Systematic geomorphologic mapping of the ridges in Synthetic Aperture RADAR (SAR) images reveals that the orientation of ridges is globally E–W and the ridges are more common near the equator than the poles. Comparison with a global topographic map reveals the equatorial ridges are found to lie preferentially at higher-than-average elevations. We conclude the most reasonable formation scenario for Titan's ridges is that contractional tectonism built the ridges and thickened the icy lithosphere near the equator, causing regional uplift. The combination of global and regional tectonic events, likely contractional in nature, followed by erosion, aeolian activity, and enhanced sedimentation at mid-to-high latitudes, would have led to regional infilling and perhaps covering of some mountain features, thus shaping Titan's tectonic landforms and surface morphology into what we see today.

1. Introduction

The Cassini spacecraft's 2.17 cm RADAR instrument has revealed that Titan has diverse geological processes, in many ways like Earth (Elachi et al., 2005; Lopes et al., 2010a). These include aeolian (Lorenz et al., 2006; Radebaugh et al., 2008, 2010; Savage et al., 2014), fluvial (Lorenz et al., 2008; Burr et al., 2009, 2013; Langhans et al., 2012), lacustrine (Stofan et al., 2007; Hayes et al., 2008; Lorenz et al., 2014), cryovolcanic (Lopes et al., 2007, 2013), and tectonic processes (Radebaugh et al., 2007, 2011; Solomonidou et al., 2013). These processes have formed and shaped ubiquitous, Earth-like surface features on Titan. The features that are RADAR bright as seen by Cassini's Synthetic Aperture RADAR (SAR) with relatively high topography have been called mountains (Radebaugh et al., 2007; Barnes et al., 2007; Mitri et al., 2010) and hummocky terrains (Lopes et al., 2010a). Some mountainous areas, in particular mountain ridge belts that are long and curvilinear in morphology, have been interpreted to be related to tectonic processes (Radebaugh et al., 2007, 2011; Mitri et al., 2010; Paganelli et al., 2010; Solomonidou et al., 2013; Liu et al., this issue). Possible tectonic landforms can be examined in geomorphological and structural mapping through analysis of the highest-resolution (350 m/pixel) Cassini SAR images, obtained beginning in 2004 (Elachi et al., 2005). These images can be used to determine the origin of the mountains, as contractional fold and thrust belts, normal or reverse faults.

Analyzing topographic data and undertaking global mapping of surface features are the keys to testing a possible tectonic contribution to shaping Titan's surface (Moore and Pappalardo, 2011). Although few researchers have undertaken geomorphologic mapping of Titan's mountain ridges (Paganelli et al., 2010; Moore et al., 2014; Cook-Hallett et al., 2015), no previous work has focused on the quantitative analysis of ridge structure, orientation, and distribution at the global scale. In addition, the driving forces of tectonism and the tectonic evolutionary history of Titan remain unclear. Thus, the purpose of this study is to: (1) analyze the distribution and orientation of mountain ridges to reveal their global tectonic pattern, and (2) explore the correlations between ridges and their regional elevations (Lorenz et al., 2013) and (3) consider the implication of these mountains for Titan's surface evolution history. In this paper, we first discuss current understanding of geological process related to Titan's mountains. Then, we describe our global structural mapping procedure on SAR images and pre-

* Corresponding author.
E-mail address: zacycliu@asu.edu (Z.Y.-C. Liu).

http://dx.doi.org/10.1016/j.icarus.2015.11.021
0019-1035/© 2015 Elsevier Inc. All rights reserved.

sent the results of ridge distribution and orientation. Finally, the distribution of ridge elevations are evaluated and tested statistically.

2. Geological background

2.1. Titan's interior structure

To be able to generate the observed mountain ridge belts through tectonism, sufficient internal energy is required to produce solid-state convection within the ice shell. This is believed to occur, in the stagnant lid regime (Tobie et al., 2006; Mitri and Showman, 2008). Furthermore, measurement of the tidal Love number k_2 reveals a relatively large response of the gravity field to the tidal field of Saturn, indicating the presence of a subsurface ocean (Iess et al., 2012). The onset of convection depends mainly on the rheology of the water ice and the composition of subsurface ocean. Mitri and Showman (2008) demonstrated that for the expected heat flux from the interior, thermal convection in the ice shell of Titan could cause repeated episodes of extensional and compressional tectonism. However, Titan's tectonics may alternatively be driven by tidal forces and the change of the satellite's figure through the mechanisms of internal cooling and rotational and orbital evolution (e.g., despinning, polar wander) without requiring a high heat flux produced in the interior (Collins et al., 2009; Moore and Pappalardo, 2011). Mitri et al. (2010) developed a thermal model of Titan's interior showing that Titan probably experienced global contraction during its secular cooling, which can produce tectonic features on the surface.

Titan's relatively low moment of inertia (MoI $\sim$ 0.34) measured by the Cassini spacecraft (Iess et al., 2010) indicates that Titan's interior may be only partially differentiated. This would indicate that Titan hasn't undergone strong internal heating. Nimmo and Bills (2010) established a model for Titan's long-wavelength topography consistent with the observed tidal Love number and moment of inertia (Zebker et al., 2009); they suggest that Titan's ice shell has thickness of $\sim$100 km and is conductive today, significantly limiting the amount of present-day geological activity expected. In addition, the strong inverse correlation between gravity and topography at long wavelengths led. Hemingway et al. (2013) to conclude Titan's ice shell is rigid and that relatively small topographic features on the surface are associated with large roots extending into the underlying ocean. They suggest that Titan's geological activity is limited at present day and Titan may be even less centrally condensed than previously thought. However, O'Rourke and Stevenson (2014) found that thermal convection couldn't realistically remove all of Titan's radiogenic heating to present day, so a partially differentiated Titan is unstable over geologic time. They concluded that Titan must be internally differentiated, and the discrepancy in the MoI could be explained by Titan having a mantle of serpentinized (hydrated) rock. Moreover, Baland et al. (2014) demonstrated that the measured obliquity of Titan (Stiles et al., 2008) indicates a higher degree of internal differentiation than expected from the moment of inertia inferred by the quadruple moment of the gravity field measurement (Iess et al., 2010). In sum, the hypotheses related to Titan's internal structure, crustal thickness, the degree of differentiation, and thermal evolution are still debated. Thus, an analysis of their structural and geographic patterns would help us understand Titan's evolutionary and geological history.

2.2. Titan's mountains

Titan's mountains have a variety of morphologies, described by four general categories: (1) *ridges*: chains of hills with elongate, curvilinear/linear crests that are higher than the surrounding areas (Fig. 1a). In many regions, ridges occur in parallel groups; we call these ridge belts. (2) *Isolated blocks*: elevated blocks with rough, SAR-bright surfaces that are generally isolated (Fig. 1b). (3) *Rugged or crenulated terrains*: rough mountains that have likely experienced erosion and have hummocky morphologies, wherein multiple adjacent peaks extend across vast regions (Fig. 1c). The crenulated nature observed in SAR is likely from the great relative elevations of these features, typically at least several hundred meters (Fig. 1c). Moore et al. (2014, 2015) pointed out that crenulated terrain generally occurs in closely spaced discrete patches, often with significant linear elongation that might be associated with tectonic deformation. Rugged and crenulated terrains are mainly located in the Xanadu region (centered at 5°S, 100°W) (Lopes et al., 2010a; Radebaugh et al., 2011; Moore et al., 2014), the first surface feature of Titan seen from Earth (Lemmon et al., 1993; Smith et al., 1996). Xanadu stands out globally as a bright feature on Titan's leading hemisphere and this brightness is the result of either compositional or textural differences in this region compared with other areas on Titan (Radebaugh et al., 2011; Langhans et al., 2013; Janssen et al., 2009, this issue). The last morphological category is (4) *massifs*: compact groups of mountainous peaks with rough, SAR-bright surfaces (Fig. 1d).

Note that Cassini RADAR altimetry, SARTopo (absolute topography with respect to the 2575 km radius sphere obtained from overlapping SAR images; Stiles et al., 2009) (Fig. 1), stereo DTM (digital terrain model) (Kirk et al., 2013), and radarclinometry data (Radebaugh et al., 2007; Liu et al., 2011) show that radar-bright mountains generally have a positive relief of several hundreds meters (Mitri et al., 2010; Kirk et al., 2013). Impact craters are also SAR bright (Fig. 1e) but have highly curved, rugged rims in contrast with the broad, open curvilinear shapes of ridges and ridge belts. Based on this difference in morphology, one can distinguish impact craters from mountainous terrains on Titan. There are only a few named impact craters, far fewer than would be expected compared to other bodies in the Solar System (Lorenz et al., 2007; Wood et al., 2010; Neish and Lorenz, 2012). The scarcity of impact craters, likely due to resurfacing inclusive of erosion and deposition or formation in marine environments (Neish and Lorenz, 2014), indicates that Titan's surface is very young, on the order of a few hundred million years old (Wood et al., 2010; Neish and Lorenz, 2012; Neish et al., this issue).

2.3. Degradation of Titan's surface

Degradation through erosion by methane rainfall plays an important role in altering Titan's surface landscapes (Collins, 2005; Burr et al., 2006; Perron et al., 2006), including mountains (Radebaugh et al., 2007). In addition, Cassini's Imaging Science Subsystem (ISS) has shown evidence that seasonal precipitation (e.g., methane rainfall) has facilitated erosion on Titan's surface (Turtle et al., 2011a, 2011b). Thus, interpreting the morphology of mountains must include the consideration of the effects of erosion.

The extent of erosion on Titan is not precisely known, but experimental work and observations suggest erosion rates somewhat slower than those on Earth. Collins (2005) originally suggested that the erosion rates on Titan were similar to those on Earth, even when the different materials and gravitation accelerations were taken into consideration. More recent work (e.g., Collins et al., 2011), however, suggests that the erosion rates are slower on Titan, perhaps by up to an order of magnitude. This experimental work is supported by observations of the degradation states of Titan's coastlines and impact craters (Black et al., 2012; Tewelde et al., 2013; Neish et al., this issue). Black et al. (2012) undertook a quantitative analysis of the shape of drainage networks on Titan,

Please cite this article in press as: Liu, Z.-Y.C., et al. The tectonics of Titan: Global structural mapping from Cassini RADAR. Icarus (2015), http://dx.doi.org/10.1016/j.icarus.2015.11.021

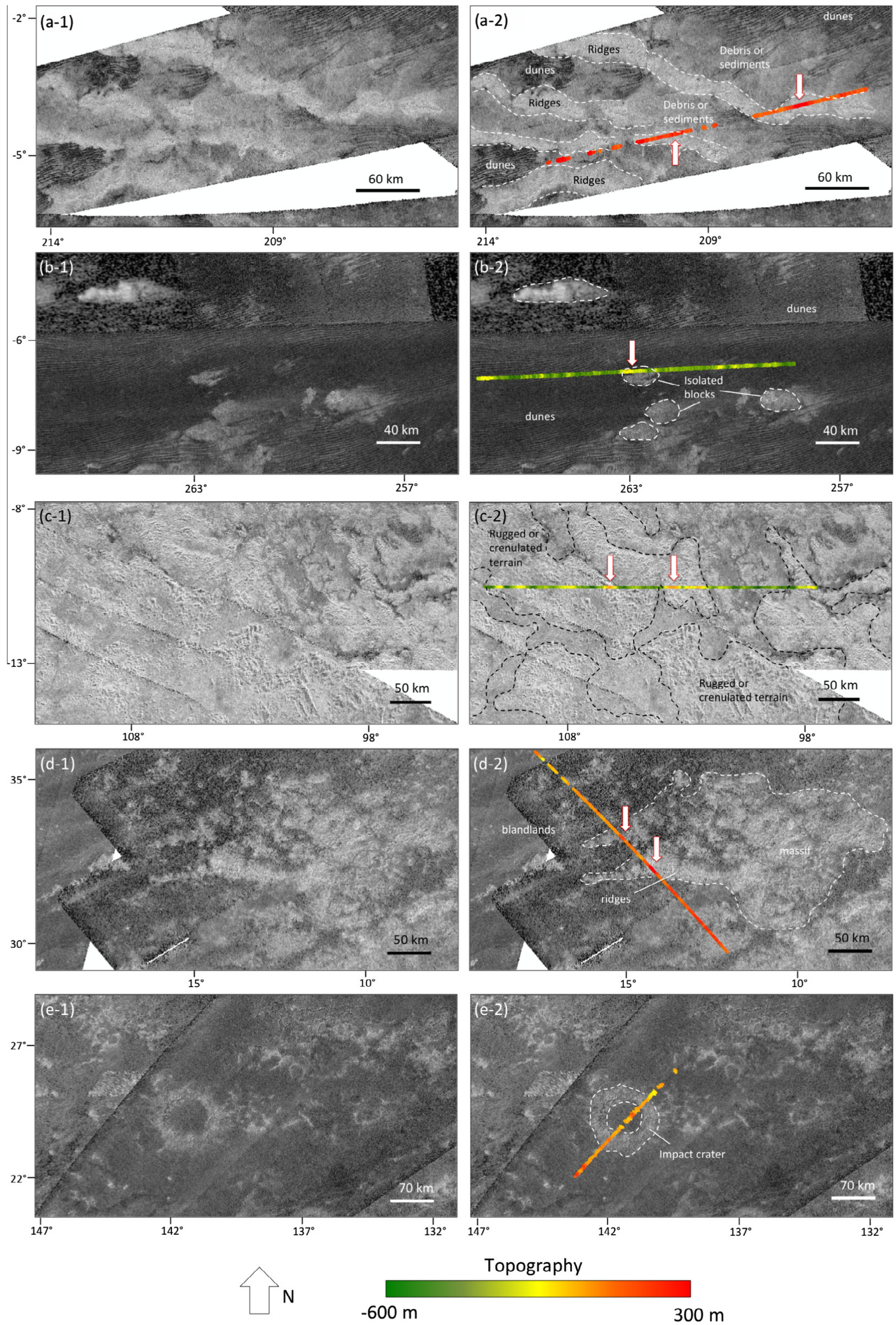

Fig. 1. Cassini Synthetic Aperture RADAR (SAR) images of mountainous surface features on Titan (first column of images) along with an annotated version and SAR topographic profiles (second column of images). The SARTopo technique obtains absolute topography with respect to the 2575 km radius sphere from overlapping SAR images (Stiles et al., 2009). White arrows indicate the highest elevations within ridge region along a SARTopo track. (a) The SAR T61 flyby swath (209°W, 4°S) shows long, SAR-bright curvilinear, multilobate ridges. SAR-dark, narrow, linear features are aeolian dunes. Dunes stop at the margins of the elevated ridge regions. Eroded debris and sediment may have accumulated between the ridges. (b) SAR T8 flyby swath (260°W, 8°S) shows multiple isolated, elevated blocks within the dune-rich area. Dunes diverge around these elevated SAR-bright blocks. (c) Rugged/crenulated ridges and eroded highlands from the SAR flyby T13 swath (100°W, 10°S). The rugged morphology is different from (a) and consists of a multitude of small hills across a broad region. The curvilinear, multilobate shapes of these rugged ridges is still recognizable even with the eroded morphology (d) T23 radar swatch shows a massif in the mid-latitude blandlands (14°W, 33°N), a compact group of mountains with rough, SAR-bright surfaces. SARTopo profile shows these features have higher elevation than the surrounding blandlands. (e) SAR T16 swath (142°W, 24°N) demonstrates how the highly curved morphology of a rugged ring of mountains on an impact crater rim differs from that of the more gently curved linear ridges in (a). Image courtesy of NASA/Cassini, north in all images is up. SARTopo profiles verify our identification of the area as elevated ridges.

the results of which show spatially averaged fluvial erosion of 0.4–9% of the initial topographic relief. Tewelde et al. (2013) analyzed the sinuosity of polar lake shorelines and concluded the erosion ranges from 4% to 31% of the initial relief. Neish et al. (2013) found that craters can be eroded by as much as 80% of their original height, and Neish et al. (this issue) found that the erosion rate must be <2×10^{-6} m/yr to retain degraded but recognizable craters in the equatorial regions, for a surface age of ~500 Myr.

The amount of erosion of mountains on Titan is unknown, as it depends on the age and original height of the mountain. But if they are of similar age to the impact craters on Titan's surface, they may be eroded by several hundred meters (Neish et al., 2013; Hemingway et al., 2013). In sum, these studies imply that fluvial erosion is not capable of completely eliminating craters or mountain ridges in most regions on Titan, though slightly higher erosion rates may erase craters in Titan's polar regions (Neish et al., this issue). In addition, ridges on Titan have likely still preserved their original trend and orientation, even in the face of erosion. Furthermore, recent studies on the degradation of impact craters (Neish et al., 2013; Schurmeier and Dombard, 2015; Neish et al., this issue) suggest aeolian infill is the main cause of the shallowness of Titan's craters, although some amount of viscous relaxation and fluvial modification (Neish et al., this issue) may have contributed to their modification. Aeolian sedimentation of Titan's equatorial ridges is not capable of altering the ridge's original trend and orientation. Thus, regardless of the erosional processes on Titan, mapping observed trends and morphologies of ridges can reveal aspects of their structural pattern.

3. Global structural mapping

3.1. Cassini SAR images

Cassini SAR images are obtained in swaths as narrow as 150 km wide and a few thousand kilometers long. The resolution of each pixel is related to the flyby trajectory, with best resolutions close to 350 m/pixel. To date, SAR images cover nearly 60% of Titan's surface. The resolution of Cassini SAR images is sufficient to map many curvilinear ridges and lineaments. The elevation data, however, are sparse in both RADAR altimetric and SARTopo data (Stiles et al., 2009; Lorenz et al., 2013). The SAR images we used here for structural mapping are from Titan flybys Ta to T84, those obtained from October 2004 to June 2012. Recent Cassini Titan flybys (T92–T95) were dedicated to monitoring its polar lakes and the transient features in Ligeia Mare (Hofgartner et al., 2014). Thus, they were obtained as strips from the polar regions to low latitudes, meaning the surface coverage of mountain belt regions did not increase significantly as a result.

3.2. Mapping with SAR images

The SAR images used to characterize Titan's surface morphologies have brightness variations that represent normalized microwave energy backscattered from the surface. SAR brightness is a function of surface slope, dielectric properties, roughness, and the amount of volume scattering (Campbell, 2002; Stofan et al., 2011). Since there are significant differences between microwave and more familiar optical wavelengths of imaging, caution should be exercised when using SAR images to map and interpret surface features.

The SAR images are obtained using a side-looking geometry. The angle at which the SAR images the target as measured from spacecraft nadir is called the look angle, θ_l. At the target, local undulations combined with the look angle create the local incidence angle, θ_i. Because of planetary curvature, the look angle does not equal the local incidence angle, an effect particularly severe for Titan due to the relatively large altitude at which imaging is performed. Based on Ford and Plaut (1993), the local incidence angle is:

$$\theta_i = \sin^{-1}\left(\frac{r+H}{r}\sin\theta_l\right) \tag{1}$$

where r is the radius of Titan (r = 2576 km) and H is the altitude of the Cassini spacecraft. Normally, for the Cassini Titan flyby data, H is about 1000–4000 km (Stiles et al., 2009) and the desired incidence angle is between 10° and 35° (Kirk et al., 2006), which makes the look angle relatively small (Ford and Plaut, 1993) typically ranging from 7° to 26°. Imaging radars with small look angles, such as Cassini SAR, enhance the topography at the expense of surface roughness information. In our structural mapping, we are more interested in topographic relief than roughness; thus, Cassini SAR images are good tools for locating and analyzing mountain ridges. The orientation of linear features relative to the SAR look direction (or azimuth) also controls the visibility of the features (Ford and Plaut, 1993) and may affect the apparent orientation of some ridges. Where the illumination is parallel to the features, there is little enhancement of the features. Where the illumination is normal to the features, topographic variations stand out. Before mapping the location and orientation of surface features, we compared multiple SAR images of the same location (when possible) to decrease the effect of illumination direction on our interpretation of ridge orientations. For the current available SAR images, about 30% of the ridge locations have more than one SAR image.

3.3. Mapping method

The geological mapping of tectonic structures can be used to interpret the types and sources of stress related to their formation (Thomas, 1988; Tanaka et al., 2010). Structural mapping enables us to determine Titan ridge origins by revealing global tectonic pattern and key morphologies. In this study, we mapped the distribution, length, and orientation of SAR-bright ridges by tracing ridge crests (Fig. 2) as lineaments in ESRI's ArcGIS. The SAR-bright ridges we mapped are features that are topographically high and rugged, exhibiting evidence of topographic shading (Fig. 1) (Radebaugh et al., 2007; Mitri et al., 2010; Kirk et al., 2013). We mapped the ridges in the equatorial and mid-latitude regions (60°N–60°S) using a modified version of the USGS Titan ArcGIS project with a geographic projection. For the surface features in the polar regions (60°N–90°N; 60°S–90°S), we mapped ridges on a polar projection. All features were identified in the SAR images as ridges where SAR-bright materials are paired with SAR-dark, which we interpret is along the crest of the ridge. These features were mapped in ArcGIS as a shapefile with a polyline in ArcMap that contains direction (azimuth) and length of the landform. Each feature was mapped using ArcMap embedded COGO (managing coverage and coordinate geometry) tools. COGO incorporates accurate coordinate geometry to create objects in ArcMap and to account for the distortions caused by the different projections. The lengths and azimuths of the mapped features are used to make rose diagrams to evaluate ridge orientation and distribution.

4. Results

4.1. Ridge morphologic types

We identified three types of mountainous ridges based on the length, segmentation, and degree of dissection (Fig. 2). We classified ridges longer than 100 km as 'long and continuous' ridges (red symbols) (Fig. 2a). Ridges shorter than 100 km were classified

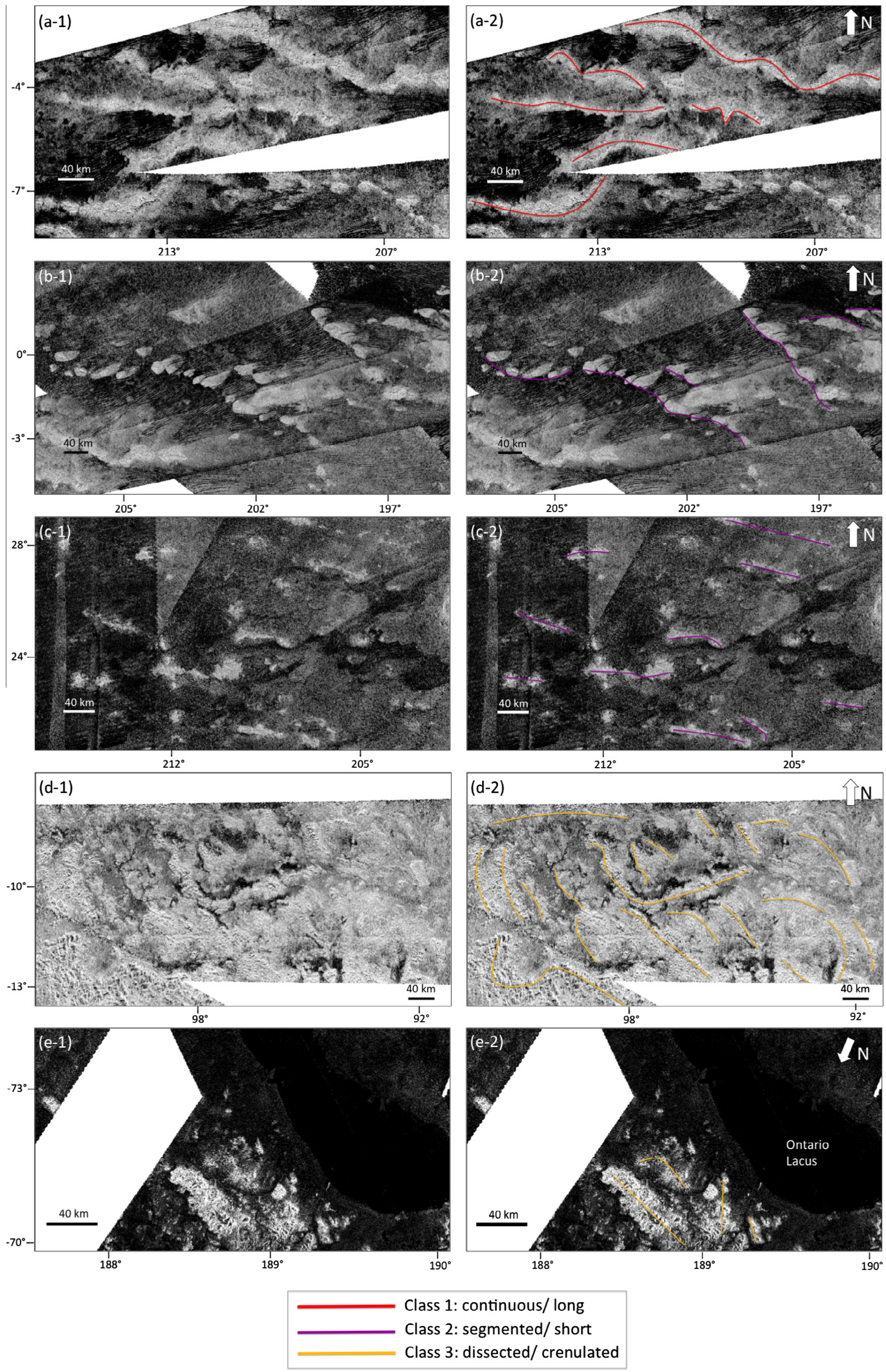

Fig. 2. The classification for three classes of mapped features and their symbols are shown. First column images are Cassini SAR; second column images contain the interpretive version showing mapped units. The SAR image mosaic shows examples of (a) the long/continuous ridges (red lines; class 1) in the equatorial region, (b) the short/segmented ridges (purple lines; class 2) in the equatorial region and (c) in the mid-latitude region (blandlands), (d) the dissected/crenulated ridges (yellow lines; class 3) in the Xanadu region and in the (e) polar region. The detailed discussion is in Section 4.1. SAR image mosaic is courtesy of NASA/Cassini. (For interpretation of the references to color in this figure legend, the reader is referred to the web version of this article.)

as ‘short and segmented’ ridges (purple) (Fig. 2b and c). Rugged ridges consisted of elongate masses of hummocks forming a ridge with a dissected morphology were classified as ‘dissected and crenulated” ridges (yellow) (Fig. 2d and e). The three ridge groups in our mapping are described in the following sections. Note that we focused on mapping continuous to discontinuous mountain ridges, leaving aside the isolated, radar-bright blocks.

4.1.1. Long and continuous ridges (class 1)

Long and continuous ridges are elongate, elevated, SAR-bright features with curvilinear margins. In many regions, a series of parallel ridges forms a ridge belt (Fig. 2a). (In contrast, SAR-black linear features are sand dunes, which curve around obstacles, stop at the margins of higher elevation landforms, and branch and then merge around ridges.) A set of large, continuous ridges longer than 100 km (207°W, 4°S) in a ridge belt west of the Huygens landing site (Fig. 2a), serves as a type locale for this class of ridges. Their curvilinear morphology is comparable to the Yakima Fold Belt in Washington, USA (see the discussion in Section 5.1). The heights of the ridges are few hundred to 1000 m based on SAR topographic profiles (Stiles et al., 2009), with a few slightly higher peak elevations based on radarclinometry (Radebaugh et al., 2007; Liu et al., 2011). These ridges found in Cassini flybys T8 and T61 have closely paired bright and dark areas, indicative of radar illumination across a sharp topographic boundary, which have curvilinear margins and can be found in parallel groups of ridges. Each mapped line represents the trend of a single continuous ridge longer than 100 km. Each red line represents a single ridge crest longer than 100 km.

4.1.2. Short and segmented ridges (class 2)

Ridges shorter than 100 km are much more common than the long continuous ridges just described. Typically they form parts of much longer trends but are broken by gaps of several kilometers. Type examples of these segmented ridges lie north of the Huygens landing site (202°W, 2°S) (Fig. 2b). Segmented ridges can also be found in mid-latitude ‘blandlands’ region (or undifferentiated plains unit) (Lopes et al., 2010a, 2013, submitted for publication) (Fig. 2c). Based on the continuous trend and morphology, these segmented ridges likely used to connect to each other as longer ridges but they have been dissected by fluvial erosional processes and perhaps subsequently buried by aeolian processes, resulting in the current, segmented morphologies. Due to their geomorphological difference from class 1 ridges, here we map the multiple segmented ridge crest using a purple line (Fig. 2b and c). Each segment must be shorter than 100 km to be included in this class; gaps between adjacent segments are as small as 1 km. Compared with the longer ridges of class 1, the class 2 segmented ridges are more common and are distributed all across Titan, while the continuous class 1 ridges are only found in the equatorial regions.

4.1.3. Dissected and crenulated ridges (class 3)

The Xanadu region (centered at 5°S 100°W) is heavily eroded by fluvial channels and contains dry basins filled with smooth, SAR-dark material, perhaps sediments from past lakes (Radebaugh et al., 2011; Fig. 2d). Xanadu’s impact crater density is the highest on Titan, and it is believed to be the oldest province on the satellite (Wood et al., 2010; Radebaugh et al., 2011). Mountains in Xanadu have multiple, adjacent, mountain peaks scattered across the terrain to create a rugged, dissected, and crenulated landscape (Radebaugh et al., 2011; Langhans et al., 2013; Moore et al., 2014). Many isolated or semi-isolated mountains form linear or arcuate, ridge-like patterns. Ridge relief within Xanadu reaches over 2000 m (Radebaugh et al., 2011), yet the overall elevation of Xanadu is low compared to surrounding sand seas (Radebaugh et al., 2011; Lorenz et al., 2013). Even with the complexity of the morphologic features in Xanadu, the trends of arcuate and aligned mountain ridges are still recognizable at Cassini SAR resolution. In Fig. 2d, multiple rugged and arcuate ridges are mapped as ‘dissected and crenulated’, using a yellow line. Outside the Xanadu province, rugged ridges can also be found at (75°W 50°N) and in a few places in the polar regions (Fig. 2e).

4.2. Differences from previous mapping works

Several previous studies have mapped and classified surface features on Titan (e.g., Lopes et al., 2010a, 2010b; Moore et al., 2014) and a few specifically focus on elevated mountainous features (e.g. Paganelli et al., 2010; Cook-Hallett et al., 2015). The recent work of Cook-Hallett et al. (2015) produced similar global mapping of mountains and hills but embraced a different morphologic classification system and mapping method than this study. The classifications of mountains used in Cook-Hallett et al. (2015) are mountain chains, hills, and Xanadu mountains. Mountain chains are identified in Cassini RADAR by a bright-dark pairing, similar to our class 1 ridges (long and continuous) while hills form teardrop shapes within the dunes, displaying nonlinear, marbleized variegation of bright-dark pairing (Cook-Hallett et al., 2015). Xanadu mountains are defined by the rugged terrains in the Xanadu region, which are similar to our class 3 ridges (dissected and crenulated). However, in our mapping we show that rugged ridges can also be found in other regions on Titan (as discussed in Section 4.1.3). Moreover, a set of class 1 equatorial ridges (207°W, 4°S) with curvilinear morphology identified in our mapping (see Section 4.1.1) was classified as hills in Cook-Hallett et al. (2015).

Cook-Hallett et al. (2015) mapped mountain units as polygons that incorporated all of the mountain mass, while we focused on polylines along the ridge crests. They developed an algorithm to determine the orientation of the mapped polygon units based on the polygon long axis, while our mapping of ridge lineaments focuses on the structural aspects of the mountains (e.g., Tanaka et al., 2010; Watters et al., 2009; Byrne et al., 2014; Klimczak et al., 2015).

4.3. Global structural map

A global structural map, showing ridge orientations mapped on SAR swaths, is presented in Fig. 3. The mapped units are limited to locations where there is SAR coverage, so there are likely many ridges that remain unobserved outside of the swath boundaries. A total length of 85,388 km of ridge features of all types were identified and mapped. The pattern of E–W orientation is obvious globally, both at equatorial and polar regions. The continuous (length > 100 km) ridges (red) are mainly located in the equatorial regions and the dissected/crenulated ridges (yellow) are mainly in the Xanadu province. Since the mapped features contain information on direction (azimuth) and length, we use these parameters to analyze the distribution of the structures and to examine the tectonic pattern in rose diagrams.

4.4. Ridge distribution and orientation

To analyze the distribution of the mapped ridges, we set up a numeric indicator, the ridge density (RD):

$$\mathrm{RD} = \frac{L}{A} \tag{2}$$

where L is total mapped ridge structure length and A is the SAR coverage area. The unit of RD is 100 km^{-1}. A high RD means there are more mapped structures or ridges per unit area. We divide Titan’s surface into six 30° latitude bands: (1) *North Pole (NP)*: 90°N–60°N, (2) *North Mid-latitude (NM)*: 60°N–30°N, (3) *North*

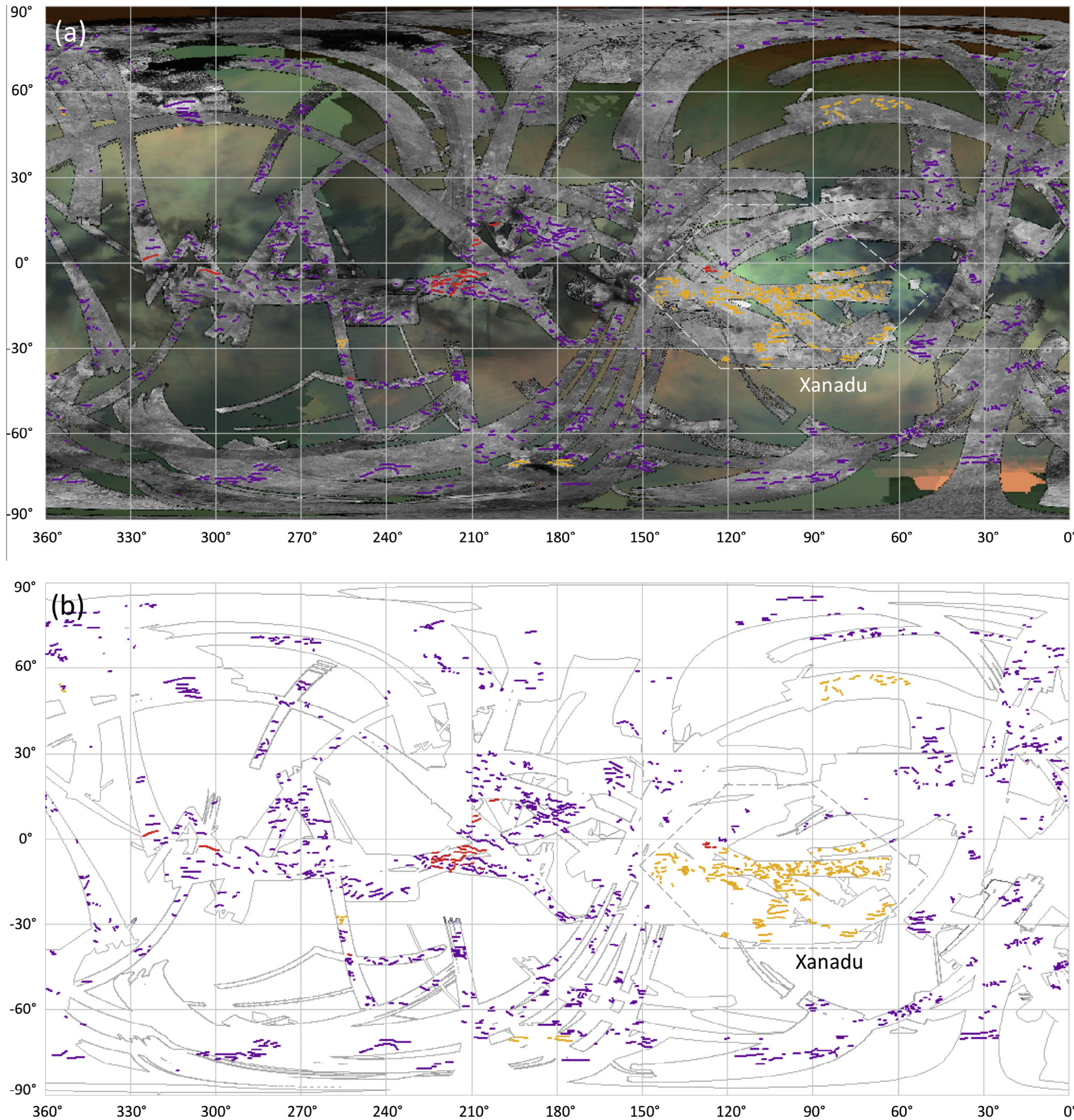

Fig. 3. (a) Global structural map of Titan with Cassini SAR images overlain on a background image from the Cassini Visual and Infrared Mapping Spectrometer (VIMS). (b) Titan structural map with Cassini SAR footprint background. Each line is a traced strike of an individual ridge (see the discussion in Sections 3.3 and 4.3). The Xanadu region is outlined by a gray dashed line. Basemap courtesy NASA/JPL/USGS. The VIMS image represents real color information with red assigned to 2.7 μm, green to 2.0 μm, and blue to 1.3 μm (Brown et al., 2004). (For interpretation of the references to color in this figure legend, the reader is referred to the web version of this article.)

Equatorial (NE): 30°N–0°, (4) *South Equatorial (SE)*: 0–30°S, (5) *South Mid-latitude (SM)*: 30°S–60°S, (6) *South Pole (SP)*: 60°S–90°S. The ridge density (RD) and related values within the six latitude bands are listed in Table 1. The highest RD measured is in the south equatorial (*SE*) region between 0°S and 30°S (RD = 0.33) and the RD of the north equatorial (*NE*) and south mid-latitude (*SM*) (RD = 0.18, 0.19 respectively) regions are generally larger than at the poles.

Ridge orientations, which are length-weighted by dividing segments of constant orientation into 1 km intervals, are plotted in 30° latitude interval bands as rose diagrams (Fig. 4). The dominant orientation of ridges in both equatorial and polar regions is E–W. Note that comparing our results with the mapping results of Cook-Hallett et al. (2015), both studies reveal a tectonic pattern of E–W oriented ridges within 30° of the equator. Because of different mapping methods (as discussed in Section 4.2), Cook-Hallett et al. (2015) also found a tectonic pattern of E–W oriented ridges within 30° of the equator but they concluded that the mountains were oriented N–S between 60° latitude and the poles, while we found a tectonic pattern of E–W globally. Consequently, this discrepancy leads to different conclusions regarding the mechanisms responsible for tectonism on Titan (see Section 5.2).

Please cite this article in press as: Liu, Z.-Y.C., et al. The tectonics of Titan: Global structural mapping from Cassini RADAR. Icarus (2015), http://dx.doi.org/10.1016/j.icarus.2015.11.021

Table 1
Ridge density (RD) data of mapped tectonic features.

Region	Latitude (°)	Total SAR area (km^2)	SAR coverage (%)	Total ridge length (km)	Ridge density (RD) (100 km^{-1})
North Pole (NP)	60–90°N	3,868,779	69	3085	0.08
North Mid-lat (NM)	30–60°N	7,569,966	50	8662	0.11
North Equator (NE)	0–30°N	12,519,518	60	20,298	0.18
South Equator (SE)	0–30°S	11,453,532	55	37,357	0.33
South Mid-lat (SE)	30–60°S	6,114,171	40	11,399	0.19
South Pole (SP)	60–90°S	3,823,641	68	4587	0.12

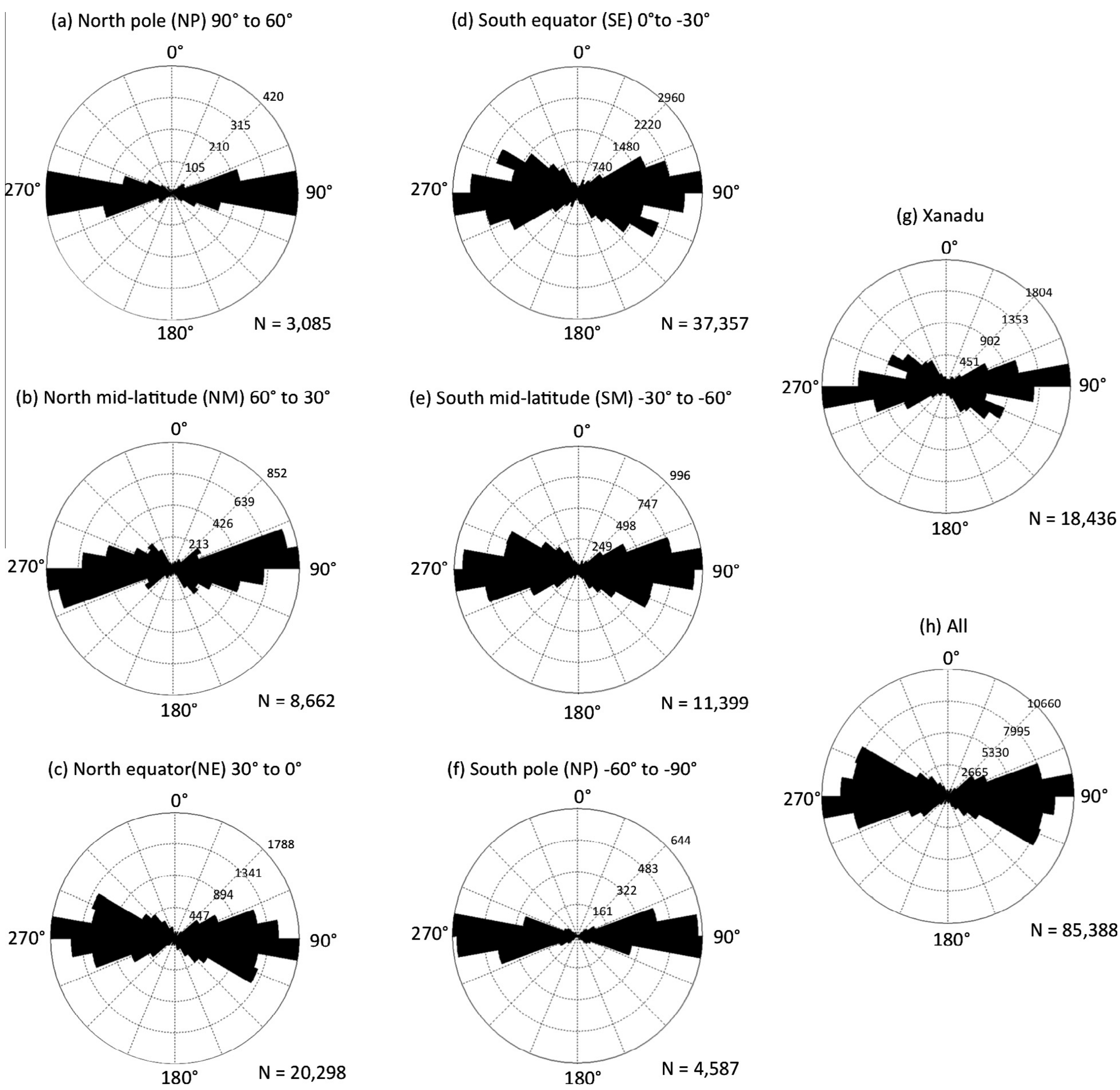

Fig. 4. Lineament azimuth distributions weighted by length. Rose diagrams are plotted in six 30° latitude interval bands with length scales. *N* represents the total length (km) of measured ridges within each 30° latitude region. (a) *North Pole (NP)*: 90°N–60°N, (b) *North Mid-latitude (NM)*: 60°N–30°N, (c) *North Equatorial (NE)*: 30°N–0°, (d) *South Equatorial (SE)*: 0–30°S, (e) *South Mid-latitude (SM)*: 30°S–60°S, (f) *South Pole (SP)*: 60°S–90°S, (g) *Xanadu*: boundary defined in Fig. 4, and (h) *All*: all mapped ridges. E–W dominant orientation can be seen with a more scattered trend between 30°N and 60°S (*NE, SE, SM*). Other regions (*NP, NM, SP*) show clearer E–W dominant orientation only. See discussion in Sections 4.4 and 5.1.

4.5. Elevation distribution

4.5.1. The elevation of Titan's ridges

A global topographic map of Titan has been produced by Lorenz et al. (2013), in which SARTopo (Stiles et al., 2009) and altimetry data were used to construct a global gridded 1 × 1° elevation map (Fig. 3 in Lorenz et al., 2013; see Fig. 5 in this paper). Topographic data are sparse, and most of the map (90%) is based on elevations interpolated between widely spaced data using a spline algorithm. Elevations range from −1700 m to 520 m (below a

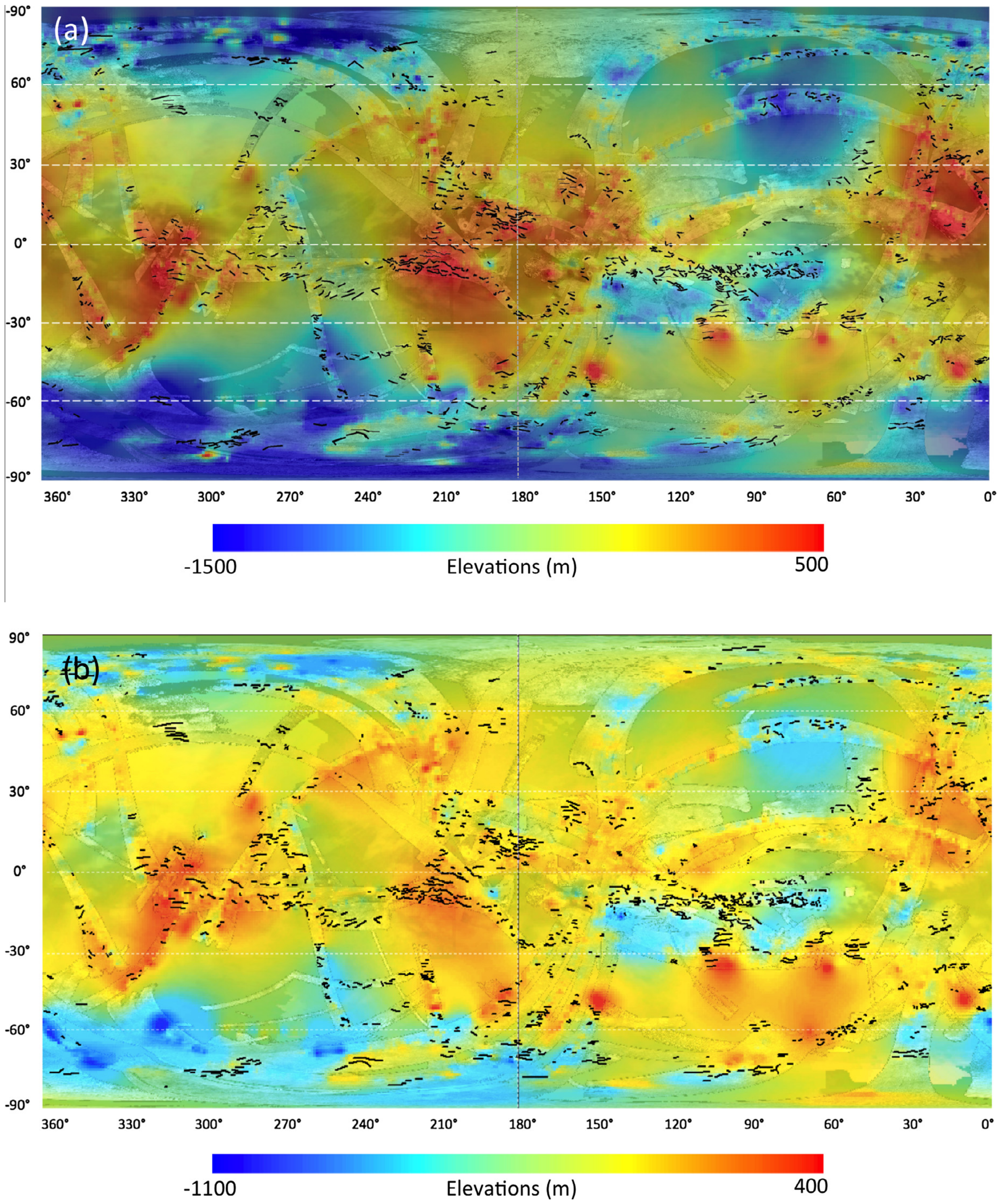

Fig. 5. (a) Titan's ridges (black lines) plotted on a global topographic map (Lorenz et al., 2013). Elevation uncertainty is ~100 m. The ridges are concentrated in topographically high regions. Cassini SAR swaths are shown shaded. (b) Geoid subtracted topographic map of Titan (see Section 4.5).

2575 km sphere). This global topographic map allows us to examine the correlation between elevation and ridge belts.

We overlay our structural map (Fig. 3) onto the topographic map in Fig. 5a. All mapped structures are shown in black. The tendency of most ridges to lie at higher elevation (red[1]) is apparent, but large areas have poorly constrained elevations. To test this correlation more rigorously, we sorted the ridges into elevation bins of 100 m, ranging from −1500 m to 500 m, where the zero elevation is the 2575 km radius sphere, and compared the ridge elevations with a histogram of Titan's global topography (Fig. 6a), following the procedure of Neish and Lorenz (2014) who examined the elevation distribution of Titan's impact craters. Iess et al. (2010) showed that Titan's gravity field is consistent with a hydrostatically relaxed body shaped by tidal and rotational effects, making it slightly oblate. Thus, it is necessary to subtract an oblate spheroid from the topography to obtain the geopotential (Fig. 5b). The geopotential is composed of the sum of the gravitational potential produced by the monopole potential, the tidal potential due to Saturn, and the rota-

[1] For interpretation of color in Fig. 5, the reader is referred to the web version of this article.

Please cite this article in press as: Liu, Z.-Y.C., et al. The tectonics of Titan: Global structural mapping from Cassini RADAR. Icarus (2015), http://dx.doi.org/10.1016/j.icarus.2015.11.021

tional potential (Iess et al., 2010). After subtracting the oblate spheroid defined in Iess et al. (2010), we again sorted the ridges into elevation bins of 100 m in size (Fig. 6b). In both cases (global topography and geoid subtracted topography), the histogram results (Fig. 6a and b) show that the elevation of ridges is skewed toward higher elevations with respect to Titan's base level. The median elevation of ridges is about 350 m higher than the median global elevation of Titan (Fig. 6a), and 250 m higher than the median geoid subtracted elevation (Fig. 6b). This confirms our conclusion that ridge belts preferentially lie at higher elevations.

To investigate this correlation, we used a Kolmogorov–Smirnov test (KS test) which serves as goodness-of-fit technique and tests whether two one-dimensional probability distributions differ (Eadie et al., 1971). The KS test evaluates the statistic D, which quantifies the difference between the cumulative distribution function for Titan's topography, $Ft(x)$, and the cumulative distribution function for Titan's ridge elevations, $Fr(x)$, at elevation x:

$$D = sup_x|Fr(x) - Ft(x)| \tag{3}$$

where sup_x is the supremum (the least upper bound) of the set of distributions. Here, the null hypothesis is that the elevations of Titan's ridges have been drawn at random from the distribution function for Titan's global topography. For the global topographic data set (Fig. 6a), this hypothesis has a significance of $D = 0.325$, and p value = 0.02 (p value is the distribution function of the KS statistic). For the geoid subtracted topographic data set (Fig. 6b), this hypothesis has a significance of $D = 0.229$, and $p = 0.03$. Thus, the null hypothesis can be rejected with 98% and 97% confidence for global topography and geoid subtracted topography, respectively, supporting the conclusion that ridge belts lie at higher elevations.

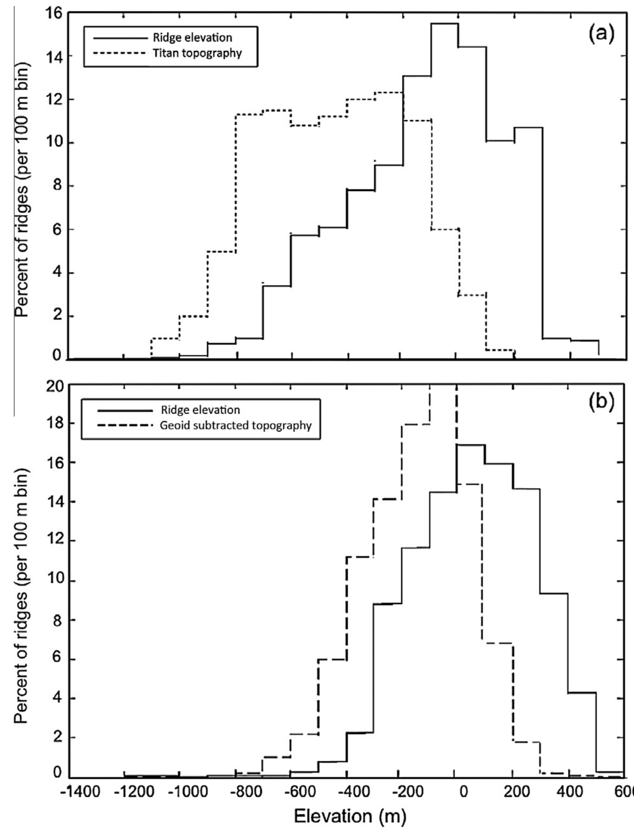

Fig. 6. (a) Histogram of Titan's global topography (dashed line) separated into 100 m bins compared to the elevations of Titan's ridges (solid line). (b) Histogram of Titan's geoid subtracted topography (dashed line) compared to the elevations of Titan's ridges. Note the tendency for ridges to lie at elevations greater than average in both cases. Detailed discussion is in Section 4.5.1.

4.5.2. Latitudinal distributions of ridge elevations

Here we examine the latitudinal distribution of ridge elevations to see if the ridges tend to lie at higher elevations at all latitudes or only at specific latitudes. We split the map of Titan into six separate latitude bands, similar to the bands chosen for ridge orientations, but each of equal area: (1) 90°N–42°N, (2) 42°N–19°N, (3) 19°N–0°, (4) 0–19°S, (5) 19°S–42°S, (6) 42°S–90°S. The purpose of separating latitudes with equal area in this analysis is to avoid the sampling bias caused by varying surface areas in equatorial and polar regions. Then we performed the same analysis as for the whole map (only global topography of Titan in Section 4.5.1) to generate the histograms, on each of these six equal-area latitude bands, comparing the global elevation in that region to the elevation of the ridges (Fig. 7a–f).

In the north pole (Fig. 7a), northern mid-latitude (Fig. 7b), southern mid-latitude (Fig. 7c), and south polar regions (Fig. 7d), it is apparent that the histograms of topography and ridge elevation are indistinguishable, meaning the ridges do not lie at broad regions of higher elevations. In contrast, at the equatorial regions (Fig. 7c and f), the distribution of ridges is skewed toward regions of higher elevations. Notably, in Fig. 7f (0–19°S), the peak in numbers of ridges found at regions of lower elevation (−250 m) is likely a result of the lower-elevation rugged Xanadu province. This analysis of latitudinal distributions of ridge elevations suggests that ridges tend to lie at higher elevations at the equator but not in the mid-latitudes or at the poles.

5. Discussion

5.1. The origin of Titan's ridges

The analysis of ridge distribution (Section 4.4) suggests that the ridges are concentrated at the equator rather than the poles. This implies that perhaps the ridges are formed preferably in the equatorial regions, or are preferentially preserved in equatorial regions. In addition, rose diagrams (Fig. 4) show the dominant orientation of ridges globally is E–W. This implies that systematic stress orientations throughout Titan's preserved surface history must have formed the tectonic structures with a preferred orientation (E–W) on Titan's surface. The similarity of the dominant ridge orientation across Titan suggests the ridges formed by a common process, where energy was concentrated and far-field stress orientations were systematic and uniform (Lopes et al., 2010a; Collins et al., 2009). However, in the three latitude bands around the equator, from 30°N to 60°S, ridges have slightly more scattered trends that can be seen in the rose diagrams (Fig. 4). This suggests that the equatorial regions have experienced a more complex tectonic history, undergoing possibly more than one stress regime.

Moreover, the rose diagram for ridges in the Xanadu region (Fig. 4) shows the same general deformation pattern as the other equatorial regions. These similarities suggests that the ridges in Xanadu formed under the same kinds of tectonic stresses, and perhaps at the same time as the other equatorial tectonic features, which is consistent with the proposed chronology of Titan's evolution and Xanadu's geologic history by Langhans et al. (2013). Langhans et al. (2013) suggest Xanadu was more recently intensely reworked and resurfaced by fluvial processes (also Radebaugh et al., 2011; Burr et al., 2009). Thus, to understand the origin and geological evolutionary history of the Xanadu province, more detailed regional structural analyses and geodynamic modeling are required.

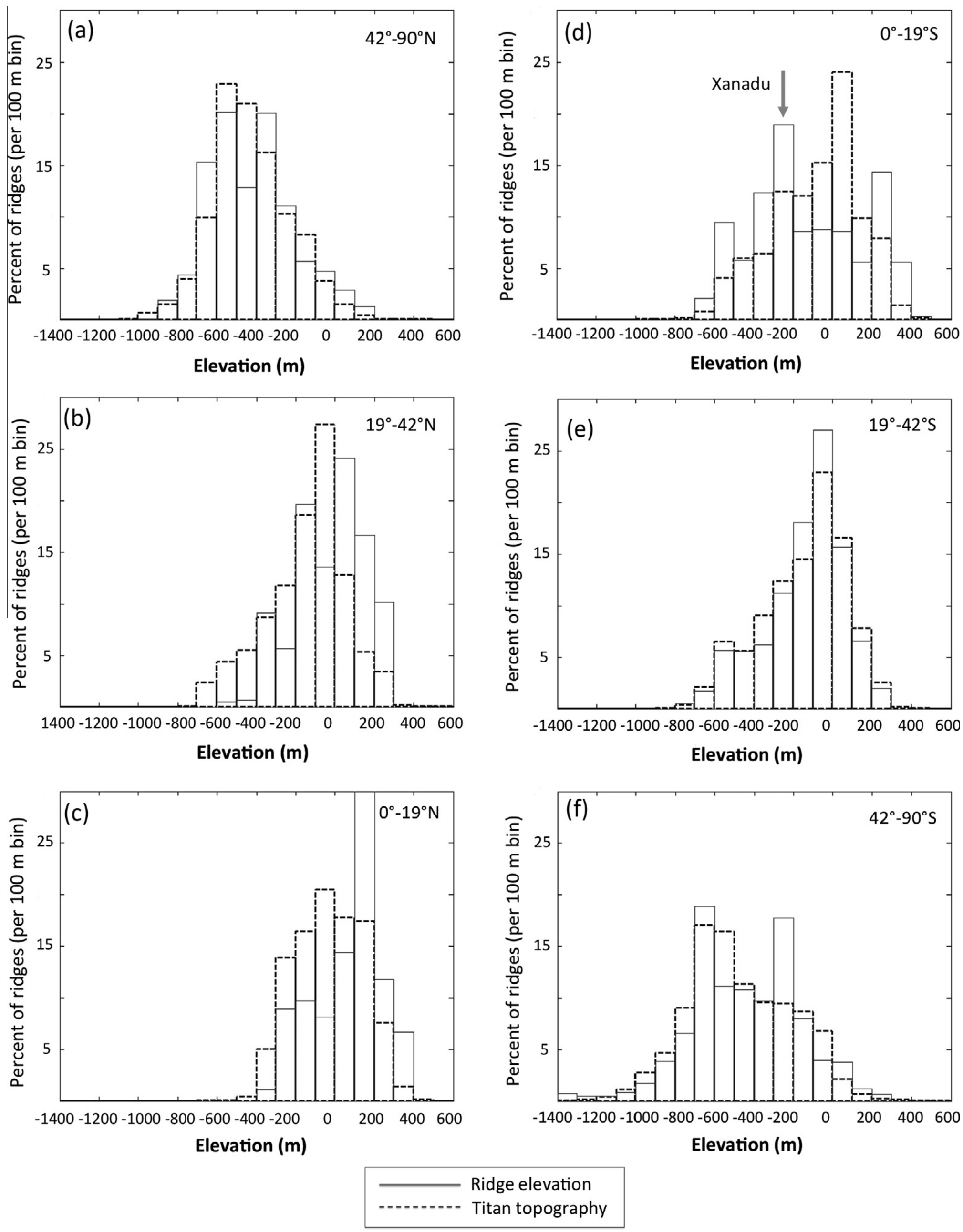

Fig. 7. Histograms of Titan's global topography (dashed line) separated into 100 m bins compared to the elevation of Titan's ridges (solid line) for each 'equal' latitude band: (a) 90°N–42°N, (b) 42°N–19°N, (c) 19°N–0°, (d) 0°S–19°S, (e) 19°S–42°S and (f) 42°S–90°S. Only equatorial regions show the tendency of ridges to lie at high elevations. The ridge peak in (c) is obvious. The ridge peak in (d) represents the lower-elevation Xanadu region. See discussion in Section 4.5.2.

On Titan, most of the ridges show linear-to-arcuate traces in plan view similar to the morphology of terrestrial fold-thrust belts, such as the Yakima Fold Belts, in Washington, USA. The Yakima Fold Belt is a series of anticlines formed by the horizontal shortening of flood basalt lavas that comprise the Columbia Plateau (e.g., Reidel, 1984). They have been compared with wrinkle ridges on the Moon (Watters, 1988). Fig. 8 demonstrates the morphological similarity (curvilinear traces and parallel groups of ridges) of Titan's equatorial ridge belts and the Yakima fold and thrust belts. The Yakima fold-thrust belts are periodically spaced (Watters, 1987), which is likely due to slip along a series of thrust faults, most of which are blind (Gerbault et al., 1999). These contractional features can be observed in the equatorial ridge belts on Titan (Fig. 8). Moreover, the average surface slope of Titan's equatorial ridge belts obtained from SARTopo profiles is <2° (Liu et al., this issue). Most average surface slopes of thrust faults and fold flanks on terrestrial planets are commonly < 15° and the slopes of mountains formed by normal faults (horsts) are commonly steeper (>45°)—where unmodified by erosion and deposition. Radebaugh et al. (2007) and Mitri et al. (2010) have previously proposed that the equatorial ridges on Titan are likely fold and/or fold-and-thrust belts based on morphologic and topographic analysis.

In sum, these observations all suggest that the ridges on Titan are tectonic origin and the equatorial ridge belts are possibly fold-and-thrust belts related to small amounts of horizontal shortening. Higher-resolution images and more detailed topographic

Please cite this article in press as: Liu, Z.-Y.C., et al. The tectonics of Titan: Global structural mapping from Cassini RADAR. Icarus (2015), http://dx.doi.org/10.1016/j.icarus.2015.11.021

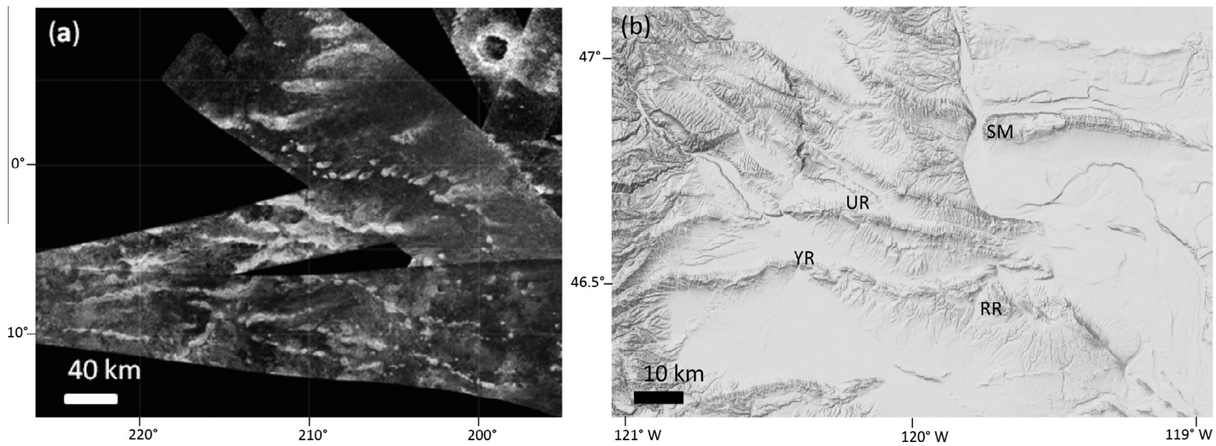

Fig. 8. The morphological similarity of Titan's equatorial ridges (a) to the Yakima Fold Belt (b) in Washington, USA. The ridges in the portion of the Yakima Fold Belt shown are the Yakima Ridge (YR), Umtanum Ridge (UR), Saddle Mountains (SM), and Rattlesnake Ridge (RR). The Yakima fold-thrusts are periodically spaced due to compressional stress; the periodic spacing is also apparent in the ridge belts on Titan. The linear-to-arcuate multi-lobate morphology of Titan's ridge belts and low surface slope also suggest they are fold-and-thrust belts comparable to their terrestrial counterparts. See discussion in Section 5.1. SAR image mosaic in (a) is from T8, T61, and T43; courtesy of NASA/Cassini. Image in (b) of Yakima Fold Belts courtesy of Google Earth terrain map.

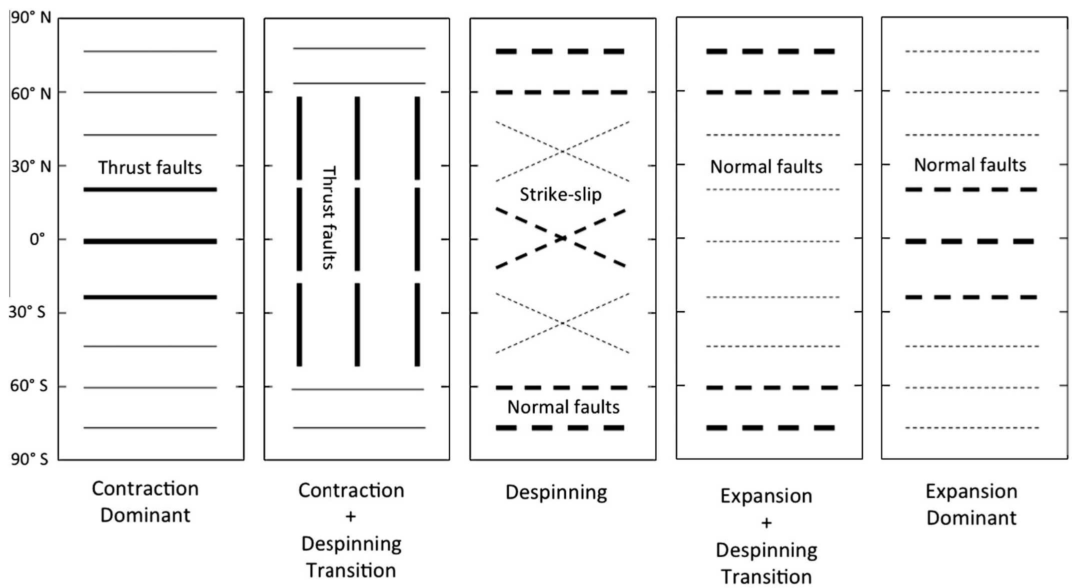

Fig. 9. The global tectonic patterns predicted by Anderson's theory for despinning, contraction, and expansion when the lithosphere is thinner at the equator, modified from Beuthe (2010). Thrust faults, normal faults, and strike-slip faults are represented with solid lines, dashed lines, and conjugate dashed lines, respectively. Faulting preferably developed where the lines are the thicker (bold lines). See Section 5.2 for detailed discussion.

data would provide further tests for the origin of the ridges on Titan, for example by locating faults or offset, though much of Titan's surface is covered in erosional debris.

5.2. Possible mechanisms to explain the global tectonic pattern

The morphological evidence from Cassini data suggests that the ridges on Titan are likely folds and thrusts (as discussed in Section 5.1); then Titan's global tectonic pattern can be examined by existing geophysical models as discussed below.

Mitri et al. (2010) constructed a global thermal model for contractional tectonism from volume change resulting from internal cooling, which built contractional folds on Titan. This model may provide enough stress to form folds and thrusts on Titan, but does not account for a global tectonic pattern. Furthermore, global volume contraction produces isotropic stress on the surface and should not produce tectonic features with preferred orientations on a global scale as we document. The global mountain and hills mapping of Cook-Hallett et al. (2015) revealed an E–W orientation near the equator and a N–S orientation at higher and polar latitudes. They interpreted the formation of ridges as due to either global contraction with a contribution of spin, in agreement with the previous hypothesis, or global expansion coupled with de-spinning if combined with a latitudinal variation in thickness of the ice shell. This model concluded the features could be produced by either extensional or compressional tectonic activity.

Beuthe (2010) proposed global contraction that incorporated thin, elastic shells with variable thickness due to latitudinal variation in solar insolation or localized tidal dissipation. He suggested a thinner equatorial lithosphere at the time of global contraction could transform the isotropic fault pattern caused by contraction into a pattern of E–W striking faults at the equatorial region (Fig. 9). He suggested that if contraction is added to despinning, the despinning pattern first shifts to thrust faults striking N–S and then to thrust faults striking E–W. If the lithosphere is initially thinner at the poles, the tectonic pattern consists of normal faults

Table 2
Summary of the scenarios that could explain the observed orientation and elevation of ridges on Titan (see detailed discussion in Section 4.2).

Scenario	Pros	Cons
Global contraction	• Capable of building ridges at higher elevation • Predicts E–W orientation • Predicts more ridges near the equator	• Global contraction would not build the ridges with observed E–W orientation (Mitri et al., 2010)
Upwelling plume	• Capable of building ridges at higher elevations	• Ridges built by upwelling plume are extensional features, such as rifts, broad topographic rise, shield volcanoes and radial features, which are not seen on the surface of Titan (Kargel, 1995) • Cryovolcanism is not prevalent on Titan
Global expansion	• Predicts E–W orientation • Predicts more ridges near the equator	• Global expansion would not build ridges at higher elevation
Fluvial erosion/sedimentation	• Capable of eroding ridges at high latitudes	• Fluvial erosion would not create observed orientation ridges
Aeolian infill	• Capable of burying ridges at the lowlands	• Most sand seas lie at equatorial highlands

striking N–S (Fig. 9). Finally, Beuthe claims the tectonic pattern caused by despinning only would produce strike-slip faults in the equatorial region (Fig. 9).

Beuthe's model of 'contraction dominant' without the despinning component is consistent with the results of our structural mapping, the analysis of rose diagrams and structure density. However, there are two problems with application of Beuthe's model on Titan. First, although faults can be properly described by elastic models by Beuthe (2010), folds and thrusts result in a visco-elastic behavior. Second, recent investigations of the comparison between the topography (shape) and gravity field by Hemingway et al. (2013) and Mitri et al. (2014) showed that the ice shell of Titan is likely thicker at the equator and thinner at the polar regions, opposite to the latitudinal variations of ice shell in Beuthe's model. Therefore, future work with improved geodynamic modeling is required to fully explain the observations.

5.3. Implications for tectonic evolution of Titan

The main conclusions of our study are: (1) ridges have an E–W orientation globally, and (2) they preferentially lie at higher-than-average elevations in the equatorial region. We explore several scenarios that could explain these correlations (Table 2).

Contraction is capable of building ridges at higher elevations and thickening the lithosphere. In addition, contraction with large, localized strain through volume change (Mitri et al., 2010) and/or global contraction (Beuthe, 2010) on Titan is capable of generating the elevated ridges striking E–W. Convective upwelling or plumes are also capable of generating locations of higher elevations. On icy satellites, convective plumes may allow melt to rise to the surface and erupt to form cryovolcanoes (Kargel, 1995; Lopes et al., 2010b). However, topographic ridges related to upwelling plumes are typically extensional features, such as horsts and grabens, rifts, broad topographic rises, and radial fractures which have not commonly been identified on Titan. In addition, the orientation of these extensional features would be radial and would not have a consistent global trend. Thus, upwelling plumes and cryovolcanism fail to explain the observations. Global expansion of the ice shell (Nimmo, 2004) is capable of building ridges striking E–W (Beuthe, 2010) (Fig. 9). However, expansion due to volume change would not build ridges at higher elevations. Instead, such tectonic features would accumulate extension in a manner similar to mid-ocean ridges on Earth (e.g., Prockter et al., 2002), which have not been identified on Titan.

It is possible that Titan's mountains were formed with a different orientation, and were later altered by fluvial erosion, which is known to create ridges between valleys as seen in the lowlands near Titan's poles (Barnes et al., 2007). Erosion can also alter an initially heavily cratered landscape, creating a plain with scattered, elevated blocks and crater rim remnants (Moore and Pappalardo, 2011; Moore et al., 2014; Neish et al., this issue). However, pure fluvial erosion would not create ridges that are regionally and globally consistent, linear, with unidirectional or dual-directional orientations, nor would it explain the location of ridges at higher elevations. Similarly, fluvial sedimentation is capable of burying ridges in the lowlands but sedimentation would not create ridges with consistent E–W orientations, so this fails to explain the observations.

As for aeolian erosion and sedimentation, summative wind directions are thought to be westerly near the equator when the greatest transportive/erosive strengths are found (Tokano, 2010; Charnay et al., 2015), consistent with the orientations of ridges. However, the ridges are globally oriented E–W even at mid-to-high latitudes where winds are not expected to be as strong. Additionally, dune orientations appear consistent with the present-day wind regime (e.g. Charnay et al., 2015), with the possible exception of some features which may be still adjusting to the Croll–Milankovich cycles in Titan's climate (e.g. Hayes et al., 2012; Ewing et al., 2015), a ~50,000 year timescale, and Barnes et al. (2008) suggest that the sand-free interdune regions imply active sand transport today. Thus it seems evident that dune formation/maintenance is presently active and is most likely more recent than ridge-building everywhere on Titan. Moreover, there are equatorial locations where dune orientations differ up to tens of degrees from mountain ridge orientations, so it is not likely that the wind formed the ridges through purely erosive processes. That more ridges are found near the equator, at high elevation, could be the result of burial of a global population of ridges by aeolian sediment at lower-elevation regions, which are mostly at mid-to-high latitudes. Most sands lie in the equatorial highlands, where dune sedimentation is occurring (Radebaugh et al., 2008; Savage et al., 2014), though an unknown amount of sand could also be present at the mid-latitudes, transported by fluvial or aeolian processes (Lopes et al., submitted for publication). Additionally, other sedimentary processes may have acted to bury surface features, especially at the mid-latitudes (Lopes et al., submitted for publication).

Overall, the most reasonable interpretation for the formation of ridges on Titan at regions of generally high elevations is that contractional tectonism built the ridges and thickened the icy lithosphere, causing regional uplift. Other interpretations, such as cryovolcanic rises, extensional tectonism, fluvial erosion, and aeolian infill, fail to explain all of the observations.

In addition, the observation that ridges tend to lie at higher elevations is only true near the equator. If ridges in both equatorial and polar regions had a similar formation mechanism and both stood at higher elevations when formed, this may imply that fluvial erosion and sedimentation in the polar regions act to fill in the lowlands and flatten the topography. This may explain why ridge

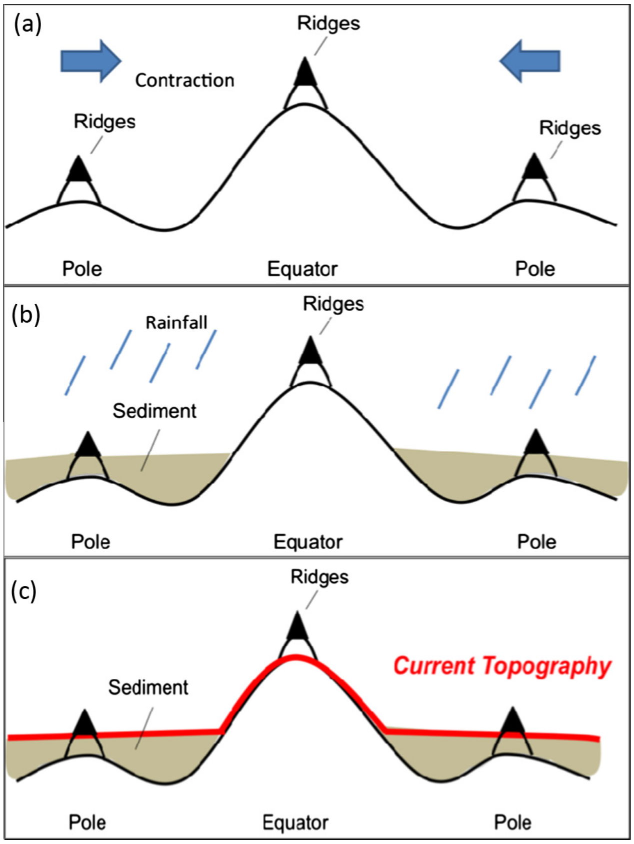

Fig. 10. Model for formation of Titan's ridges and surface evolution. (a) The schematic diagram shows that contraction built ridges at higher elevations. (b) Fluvial erosion and deposition followed and filled in the lowlands at higher elevations, which means the ridges lie at higher elevations at the equator only. (c) Finally, the red line represents current, broadly averaged topography (individual ridges are not included). Gray areas represent sediment; black triangles represent ridges. Detailed discussion is in Section 5.3. (For interpretation of the references to color in this figure legend, the reader is referred to the web version of this article.)

elevations do not sit at higher-than-average elevations at the poles (Fig. 7). Alternatively, the ridges could follow the same elevation distribution in each latitude band, but still be biased to high elevations globally because there are more ridges at low latitudes where the average elevation is greater.

Thus, all these observations would suggest a landscape evolution in which global contraction has built ridges striking dominantly E–W, and more recently fluvial erosion and sedimentation reduced the topographic differences by filling in the lowlands at high latitudes. This scenario is shown schematically in Fig. 10. The interplay of contractional tectonism, erosional and sedimentary processes have likely created and shaped the current topography we see on Titan today. Notably, this scenario is consistent with the study of Choukroun and Sotin (2012) who suggested that the global shape of Titan may be explained by subsidence at the polar regions associated with the substitution of ethane into methane clathrates.

6. Summary

Global structural analysis leads us to conclude that the origin of most ridges on Titan is tectonic. The gently arcuate morphology of ridges with very low-angle surface slopes indicates the ridges are likely contractional structures, i.e., thrust sheets and folds. If so, the combination of observations suggests that the most likely mechanism to produce the E–W ridges on Titan is contraction through volume change of Titan's interior (Beuthe, 2010; Mitri et al., 2010). An inventory of all ridges seen in Cassini SAR data reveals that the dominant orientation of ridges at all latitudes on Titan is E–W. The ridges are also more abundant at the equatorial regions, which suggests that tectonic activities were more intense near the equator. The Xanadu province has an overall similar tectonic pattern to other equatorial regions.

Comparisons with Titan's topography reveal that Titan's ridges preferentially lie at higher-than-average elevations near the equator. The most reasonable explanation for this correlation is that contractional tectonism built the ridges globally, though preferentially at equatorial regions, and then fluvial erosion, sedimentation and eolian activity followed. At regions of lower elevation, at mid-to-high latitudes, erosion and sedimentation led to regional infilling and perhaps covering of some mountain features. Seasonal and climatic changes and their interactions with the regional topography may have also affected the distribution and erosion of the ridges. This study of structural mapping and distribution analysis can provide constraints on surficial and interior evolution of Titan and may be tested by more sophisticated geodynamic models for Titan.

Acknowledgments

We wish to acknowledge the Cassini RADAR team for acquiring and processing the SAR data and we are grateful to all who developed and operate the Cassini–Huygens mission. Barry Bickmore, Simon A. Kattenhorn and Amanda L. Nahm provided invaluable discussion and encouragement. Z.Y.-C.L. was supported by a Graduate Research Fellowship at Brigham Young University, United States.

References

Baland, R.M. et al., 2014. Titan's internal structure inferred from its gravity field, shape, and rotation state. Icarus 237, 29–41. http://dx.doi.org/10.1016/j.icarus.2014.04.007.

Barnes, J.W. et al., 2007. Near-infrared spectral mapping of Titan's mountains and channels. J. Geophys. Res.: Planets 112 (E11). http://dx.doi.org/10.1029/2007JE002932.

Barnes, J.W. et al., 2008. Spectroscopy, morphometry, and photoclinometry of Titan's dunefields from Cassini/VIMS. Icarus 195 (1), 400–414.

Beuthe, M., 2010. East–west faults due to planetary contraction. Icarus 209 (2), 795–817. http://dx.doi.org/10.1016/j.icarus.2010.04.019.

Black, B.A. et al., 2012. Estimating erosional exhumation on Titan from drainage network morphology. J. Geophys. Res.: Planets 117 (E8). http://dx.doi.org/10.1029/2012JE004085.

Brown, R.H. et al., 2004. The Cassini Visual and Infrared Mapping Spectrometer (VIMS) investigation. In: The Cassini–Huygens Mission. Springer, Netherlands, pp. 111–168.

Burr, D.M. et al., 2006. Sediment transport by liquid surficial flow: Application to Titan. Icarus 181 (1), 235–242. http://dx.doi.org/10.1016/j.icarus.2005.11.012.

Burr, D.M. et al., 2009. Fluvial network analysis on Titan: Evidence for subsurface structures and west-to-east wind flow, southwestern Xanadu. Geophys. Res. Lett. 36 (22). http://dx.doi.org/10.1029/2009GL040909.

Burr, D.M. et al., 2013. Fluvial features on Titan: Insights from morphology and modeling. Geol. Soc. Am. Bull. 125 (3–4), 299–321. http://dx.doi.org/10.1130/B30612.1.

Byrne, P.K. et al., 2014. Mercury's global contraction much greater than earlier estimates. Nat. Geosci. 7 (4), 301–307. http://dx.doi.org/10.1038/ngeo2097.

Campbell, B.A., 2002. Radar Remote Sensing of Planetary Surfaces. Cambridge University Press, Cambridge, UK.

Charnay, B. et al., 2015. Methane storms as a driver of Titan's dune orientation. Nat. Geosci. http://dx.doi.org/10.1038/ngeo2406.

Choukroun, M., Sotin, C., 2012. Is Titan's shape caused by its meteorology and carbon cycle? Geophys. Res. Lett. 39 (4). http://dx.doi.org/10.1029/2011GL050747.

Collins, G.C., 2005. Relative rates of fluvial bedrock incision on Titan and Earth. Geophys. Res. Lett. 32, L22202. http://dx.doi.org/10.1029/2005GL024551.

Collins, G.C. et al., 2009. Tectonics of the outer planet satellites. Planet. Tectonics 11, 264.

Collins, G.C. et al., 2011. Resistance of water ice to fluvial abrasion and implications for erosion on Titan. Lunar Planet. Sci. 42. Abstract 2781 (Houston, TX).

Cook-Hallett, C. et al., 2015. Global contraction/expansion and polar lithospheric thinning on Titan from patterns of tectonism. J. Geophys. Res.: Planets 120 (6), 1220–1236. http://dx.doi.org/10.1002/2014JE004645.

Eadie, W.T. et al., 1971. Statistical Methods in Experimental Physics. North-Holland, Amsterdam.
Elachi, C. et al., 2005. Cassini RADAR views the surface of Titan. Science 308 (5724), 970–974. http://dx.doi.org/10.1126/science.1109919.
Ewing, R.C., Hayes, A.G., Lucas, A., 2015. Sand dune patterns on Titan controlled by long-term climate cycles. Nat. Geosci. 8 (1), 15–19.
Ford, J.P., Plaut, J.J., 1993. Magellan Image Data. Guide to Magellan Image Interpretation, vol. 1. NASA/JPL.
Gerbault, M. et al., 1999. Do faults trigger folding in the lithosphere? Geophys. Res. Lett. 26 (2), 271–274. http://dx.doi.org/10.1029/1998GL900293.
Hayes, A. et al., 2008. Hydrocarbon lakes on Titan: Distribution and interaction with a porous regolith. Geophys. Res. Lett. 35 (9). http://dx.doi.org/10.1029/2008GL033409.
Hayes, A.G. et al., 2012. Determining timescales of the dune forming winds on Titan. LPI Contributions, 1673, pp. 46–47.
Hemingway, D. et al., 2013. A rigid and weathered ice shell on Titan. Nature 500 (7464), 550–552. http://dx.doi.org/10.1038/nature12400.
Hofgartner, J.D. et al., 2014. Transient features in a Titan sea. Nat. Geosci. http://dx.doi.org/10.1038/ngeo2190.
Iess, L. et al., 2010. Gravity field, shape, and moment of inertia of Titan. Science 327 (5971), 1367–1369. http://dx.doi.org/10.1126/science.1182583.
Iess, L. et al., 2012. The tides of Titan. Science 337 (6093), 457–459. http://dx.doi.org/10.1126/science.1219631.
Janssen, M.A. et al., 2009. Titan's surface at 2.2-cm wavelength imaged by the Cassini RADAR radiometer: Calibration and first results. Icarus 200 (1), 222–239. http://dx.doi.org/10.1016/j.icarus.2008.10.017.
Janssen, M.A. et al., 2015. Titan's surface at 2.18-cm wavelength imaged by the Cassini RADAR radiometer: Results and interpretations through the first ten years of observation. Icarus. http://dx.doi.org/10.1016/j.icarus.2015.09.027.
Kargel, J.S., 1995. Cryovolcanism on the icy satellites. Comparative Planetology with an Earth Perspective. Springer, Netherlands, pp. 101–113.
Kirk, R.L. et al., 2006. A high resolution view of the Xanadu region of Titan from the Cassini RADAR. Bull. Am. Astron. Soc. 38 (Abstract 52.03).
Kirk, R.L. et al., 2013. Topographic mapping of Titan: Completion of a global radargrammetric control network opens the floodgates for stereo DTM production. Lunar Planet. Sci. 44. Abstract 2898 (Houston, TX).
Klimczak, C., Byrne, P.K., Solomon, S.C., 2015. A rock-mechanical assessment of Mercury's global tectonic fabric. Earth Planet. Sci. Lett. 416, 82–90. http://dx.doi.org/10.1016/j.epsl.2015.02.003.
Langhans, M.H. et al., 2012. Titan's fluvial valleys: Morphology, distribution, and spectral properties. Planet. Space Sci. 60 (1), 34–51. http://dx.doi.org/10.1016/j.pss.2011.01.020.
Langhans, M., Lunine, J.I., Mitri, G., 2013. Titan's Xanadu region: Geomorphology and formation scenario. Icarus 223 (2), 796–803. http://dx.doi.org/10.1016/j.icarus.2013.01.016.
Lemmon, M.T., Karkoschka, E., Tomasko, M., 1993. Titan's rotation: Surface feature observed. Icarus 103 (2), 329–332. http://dx.doi.org/10.1006/icar.1993.1074.
Liu, Z.Y.C. et al., 2011. Mountains on Titan: Height and slope analysis. Lunar Planet. Sci. 42. Abstract 2798 (Houston, TX).
Liu, Z.Y.-C. et al., 2015. Role of fluids in the tectonic evolution of Titan. Icarus (this issue).
Lopes, R.M.C. et al., 2007. Cryovolcanic features on Titan's surface as revealed by the Cassini Titan Radar Mapper. Icarus 186 (2), 395–412. http://dx.doi.org/10.1016/j.icarus.2006.09.006.
Lopes, R.M.C. et al., 2010a. Distribution and interplay of geologic processes on Titan from Cassini RADAR data. Icarus 205 (2), 540–558. http://dx.doi.org/10.1016/j.icarus.2009.08.010.
Lopes, R.M.C. et al., 2010b. Beyond Earth: How extra-terrestrial volcanism has changed our definition of a volcano. In: Canon, E., Szakacs, A. (Eds.), What's a Volcano? New Answers to an Old Question. Geological Society of Q22 America Special Paper 470, pp. 11–30.
Lopes, R.M.C. et al., 2013. Cryovolcanism on Titan: New results from Cassini RADAR and VIMS. J. Geophys. Res.: Planets 118 (3), 416–435. http://dx.doi.org/10.1002/jgre.20062.
Lopes, R.M.C. et al., 2015. Nature, distribution and origin of Titan's undifferentiated plains. Icarus (submitted for publication).
Lorenz, R.D. et al., 2006. The sand seas of Titan: Cassini RADAR observations of longitudinal dunes. Science 312 (5774), 724–727. http://dx.doi.org/10.1126/science.1123257.
Lorenz, R.D. et al., 2007. Titan's young surface: Initial impact crater survey by Cassini RADAR and model comparison. Geophys. Res. Lett. 34 (7). http://dx.doi.org/10.1029/2006GL028971.
Lorenz, R.D. et al., 2008. Fluvial channels on Titan: Initial Cassini RADAR observations. Planet. Space Sci. 56 (8), 1132–1144. http://dx.doi.org/10.1016/j.pss.2008.02.009.
Lorenz, R.D. et al., 2013. A global topographic map of Titan. Icarus 225 (1), 367–377. http://dx.doi.org/10.1016/j.icarus.2013.04.002.
Lorenz, R.D. et al., 2014. A radar map of Titan Seas: Tidal dissipation and ocean mixing through the throat of Kraken. Icarus 237, 9–15. http://dx.doi.org/10.1016/j.icarus.2014.04.005.
Mitri, G., Showman, A.P., 2008. Thermal convection in ice-I shells of Titan and Enceladus. Icarus 193 (2), 387–396. http://dx.doi.org/10.1016/j.icarus.2007.07.016.
Mitri, G. et al., 2010. Mountains on Titan: Modeling and observations. J. Geophys. Res.: Planets 115 (E10). http://dx.doi.org/10.1029/2010JE003592.
Mitri, G. et al., 2014. Shape, topography, gravity anomalies and tidal deformation of Titan. Icarus 236, 169–177. http://dx.doi.org/10.1016/j.icarus.2014.03.018.
Moore, J.M., Pappalardo, R.T., 2011. Titan: An exogenic world? Icarus 212 (2), 790–806. http://dx.doi.org/10.1016/j.icarus.2011.01.019.
Moore, J.M., Howard, A.D., Morgan, A.M., 2014. The landscape of Titan as witness to its climate evolution. J. Geophys. Res.: Planets 119 (9), 2060–2077. http://dx.doi.org/10.1002/2014JE004608.
Moore, J.M., Howard, A.D., Schenk, P.M., 2015. Landform evolution modeling of specific fluvially eroded physiographic units on Titan. Lunar Planet. Sci. 46. Abstract 2457 (Houston, TX).
Neish, C.D., Lorenz, R.D., 2012. Titan's global crater population: A new assessment. Planet. Space Sci. 60 (1), 26–33. http://dx.doi.org/10.1016/j.pss.2011.02.016.
Neish, C.D., Lorenz, R.D., 2014. Elevation distribution of Titan's craters suggests extensive wetlands. Icarus 228, 27–34. http://dx.doi.org/10.1016/j.icarus.2013.09.024.
Neish, C.D. et al., 2013. Crater topography on Titan: Implications for landscape evolution. Icarus 223 (1), 82–90. http://dx.doi.org/10.1016/j.icarus.2012.11.030.
Neish, C.D. et al., 2015. Fluvial erosion as a mechanism for crater modification on Titan. Icarus. doi: http://dx.doi.org/10.1016/j.icarus.2015.07.022 (this issue).
Nimmo, F., 2004. Stresses generated in cooling viscoelastic ice shells: Application to Europa. J. Geophys. Res.: Planets 109 (E12). http://dx.doi.org/10.1029/2004JE002347.
Nimmo, F., Bills, B.G., 2010. Shell thickness variations and the long-wavelength topography of Titan. Icarus 208 (2), 896–904. http://dx.doi.org/10.1029/2004JE002347.
O'Rourke, J.G., Stevenson, D.J., 2014. Stability of ice/rock mixtures with application to a partially differentiated Titan. Icarus 227, 67–77. http://dx.doi.org/10.1016/j.icarus.2013.09.010.
Paganelli, F. et al., 2010. Preliminary analysis of structural elements of Titan and implication for stress. Lunar Planet. Sci. 41. Abstract 2664 (Houston, TX).
Perron, J.T. et al., 2006. Valley formation and methane precipitation rates on Titan. J. Geophys. Res.: Planets (1991–2012) 111 (E11). http://dx.doi.org/10.1029/2005JE002602.
Prockter, L.M. et al., 2002. Morphology of Europan bands at high resolution: A mid-ocean ridge-type rift mechanism. J. Geophys. Res.: Planets 107 (E5), 4-1. http://dx.doi.org/10.1029/2000JE001458.
Radebaugh, J. et al., 2007. Mountains on Titan observed by Cassini RADAR. Icarus 192 (1), 77–91. http://dx.doi.org/10.1016/j.icarus.2007.06.020.
Radebaugh, J. et al., 2008. Dunes on Titan observed by Cassini RADAR. Icarus 194 (2), 690–703. http://dx.doi.org/10.1016/j.icarus.2007.10.015.
Radebaugh, J. et al., 2010. Linear dunes on Titan and Earth: Initial remote sensing comparisons. Geomorphology 121 (1), 122–132. http://dx.doi.org/10.1016/j.geomorph.2009.02.022.
Radebaugh, J. et al., 2011. Regional geomorphology and history of Titan's Xanadu province. Icarus 211 (1), 672–685. http://dx.doi.org/10.1016/j.icarus.2010.07.022.
Reidel, S.P., 1984. The Saddle Mountains; the evolution of an anticline in the Yakima Fold Belt. Am. J. Sci. 284 (8), 942–978. http://dx.doi.org/10.2475/ajs.284.8.942.
Savage, C.J. et al., 2014. Implications of dune pattern analysis for Titan's surface history. Icarus 230, 180–190. http://dx.doi.org/10.1016/j.icarus.2013.08.009.
Schurmeier, L.R., Dombard, A.J., 2015. The effects of low thermal conductivity sand on the relaxation of Titan's impact craters. Lunar Planet. Sci. 46. Abstract 2913 (Houston, TX).
Smith, P.H. et al., 1996. Titan's surface, revealed by HST imaging. Icarus 119 (2), 336–349. http://dx.doi.org/10.1006/icar.1996.0023.
Solomonidou, A. et al., 2013. Morphotectonic features on Titan and their possible origin. Planet. Space Sci. 77, 104–117. http://dx.doi.org/10.1016/j.pss.2012.05.003.
Stiles, B.W. et al., 2008. Determining Titan's spin state from Cassini RADAR images. Astron. J. 135 (5), 1669–1680.
Stiles, B.W. et al., 2009. Determining Titan surface topography from Cassini SAR data. Icarus 202 (2), 584–598. http://dx.doi.org/10.1016/j.icarus.2009.03.032.
Stofan, E.R. et al., 2007. The lakes of Titan. Nature 445 (7123), 61–64. http://dx.doi.org/10.1038/nature05438.
Stofan, E.R. et al., 2011. Cassini Image Data. Cassini RADAR Users Guide.
Tanaka, K.L. et al., 2010. Planetary structural mapping. Planet. Tectonics 11, 351–396.
Tewelde, Y. et al., 2013. Estimates of fluvial erosion on Titan from sinuosity of lake shorelines. J. Geophys. Res.: Planets 118 (10), 2198–2212. http://dx.doi.org/10.1002/jgre.20153.
Thomas, P.G., 1988. The tectonic and volcanic history of Rhea as inferred from studies of scarps, ridges, troughs, and other lineaments. Icarus 74 (3), 554–567. http://dx.doi.org/10.1016/0019-1035(88)90121-2.
Tobie, G., Lunine, J.I., Sotin, C., 2006. Episodic outgassing as the origin of atmospheric methane on Titan. Nature 440 (7080), 61–64. http://dx.doi.org/10.1038/nature04497.
Tokano, T., 2010. Relevance of fast westerlies at equinox for the eastward elongation of Titan's dunes. Aeolian Res. 2 (2), 113–127. http://dx.doi.org/10.1016/j.aeolia.2010.04.003.
Turtle, E.P. et al., 2011a. Rapid and extensive surface changes near Titan's equator: Evidence of April showers. Science 331 (6023), 1414–1417. http://dx.doi.org/10.1126/science.1201063.
Turtle, E.P. et al., 2011b. Seasonal changes in Titan's meteorology. Geophys. Res. Lett. 38 (3). http://dx.doi.org/10.1029/2010GL046266.
Watters, T.R., 1987. The Columbia and Tharsis Plateaus. Geol. Soc. Am. Abstr. Programs, vol. 19, p. 463 (abstract).

Watters, T.R., 1988. Wrinkle ridge assemblages on the terrestrial planets. J. Geophys. Res. 93 (B9), 10236–10254. http://dx.doi.org/10.1029/JB093iB09p10236.

Watters, T.R. et al., 2009. The tectonics of Mercury: The view after MESSENGER's first flyby. Earth Planet. Sci. Lett. 285 (3), 283–296. http://dx.doi.org/10.1016/j.epsl.2009.01.025.

Wood, C.A. et al., 2010. Impact craters on Titan. Icarus 206 (1), 334–344. http://dx.doi.org/10.1016/j.icarus.2009.08.021.

Zebker, H.A. et al., 2009. Size and shape of Saturn's moon Titan. Science 324 (5929), 921–923. http://dx.doi.org/10.1126/science.1168905.